Table II. Calculated Bond Lengths (Å) for the Distonic Ion $^{\bullet}CH_2OSi^{+}$ and the Singlet and Triplet States of the Biradical Neutral $^{\bullet}CH_2OSi^{\bullet}$

| bond | $^2A'$ (·+) | $^1A'$ | $^3A''$ |
|---|---|---|---|
| C-O | 1.368 | 1.340 | 1.328 |
| Si-O | 1.574 | 1.613 | 1.661 |

presence of an $SiCH_n$ ($n$ = 0-2) linkage which would be a signature of $OCSiH_2^{\bullet+}$ or $COSiH_2^{\bullet+}$ parent ions.

If the $m/z$ 58 ion is largely the distonic ion $^{\bullet}CH_2OSi^{+}$, a recovery of the biradical $^{\bullet}CH_2OSi^{\bullet}$, as either a singlet or a triplet, is expected on the basis of our theoretical results which indicate only minor differences in geometry between the distonic ion and the two spin states of the biradical (see Table II).[17] A Franck-Condon transition in the neutralization step could preferentially lead to the singlet biradical which has a geometry closer to that of the distonic ion. A similar suggestion follows from the computed values for the adiabatic and vertical ionization energies for the two spin states of the biradical to yield the distonic ion. Values of $IE_v$ = 6.41 eV and $IE_a$ = 5.75 eV were derived for the triplet, and values of $IE_v$ = 6.71 eV and $IE_a$ = 6.15 eV were derived for the singlet which is slightly more stable. So $IE_v - IE_a$ is 0.66 eV for the ionization of the triplet and only 0.56 eV for the ionization of the single biradical.

## Conclusions

1. The results of the collisional-activation and neutralization-reionization experiments together with theory are in keeping with the proposal that the $m/z$ 58 ion derived from $Si(OCH_3)_4^{\bullet+}$ corresponds to the distonic ion $^{\bullet}CH_2OSi^{+}$.

2. The results of the neutralization-reionization experiments together with theory provide evidence for the stability of the biradical $^{\bullet}CH_2OSi^{\bullet}$ and its formation from the distonic ion $^{\bullet}CH_2OSi^{+}$ by neutralization at a high collision energy of 8 keV.[33]

**Acknowledgment.** Financial support of our work by the Deutsche Forschungsgemeinschaft and the Fonds der Chemischen Industrie is appreciated. R.S. acknowledges the receipt of a visiting fellowship from the Deutscher Akademischer Austauschdienst (DAAD) and the encouragement of Dr. A. V. Rama Rao, Director, IICT, Hyderabad, India. D.K.B. is grateful to the Alexander-von-Humboldt Foundation for a Humboldt Senior Scientist Award and to H.S. for his hospitality.

(33) For the generation and characterization of other diradicals from distonic ions in the gas phase, e.g., $^{\bullet}CH_2OCH_2^{\bullet}$, see: Wesdemiotis, C.; Leyh, B.; Fura, A.; McLafferty, F. W. *J. Am. Chem. Soc.* **1990**, *112*, 8655.

# Electronic States of Benzo[*a*]pyrene. Linear and Magnetic Circular Dichroism, Polarized Fluorescence, and Quantum Chemical Calculations

**Jens Spanget-Larsen,*,† Jacek Waluk,‡ Svante Eriksson,§ and Erik W. Thulstrup⊥**

*Contribution from the Institute of Life Sciences and Chemistry, Roskilde University, P.O. Box 260, DK-4000 Roskilde, Denmark, Photochemistry and Spectroscopy Laboratory, Institute of Physical Chemistry, Polish Academy of Sciences, Kasprzaka 44/52, 01-224 Warsaw, Poland, Department of Physical Chemistry, Chalmers University of Technology, S-41296 Gothenburg, Sweden, and S-6039, The World Bank, 1818 H Street, N.W., Washington, D.C. 20433.*
*Received June 7, 1991*

**Abstract:** The carcinogen benzo[*a*]pyrene is investigated by UV and IR linear dichroism (LD) spectroscopy in stretched polyethylene, by UV magnetic circular dichroism (MCD) spectroscopy, and by fluorescence polarization spectroscopy. The combined results lead to a detailed experimental characterization of transitions in the near-UV region, with determination of polarization directions for five electronic transitions. The experimental results are compared with theoretical predictions using the PPP, CNDO/S, CNDO-SDCI, and LCOAO quantum chemical models. Excellent agreement with observed values in the low-energy region, including transition moment directions and MCD signs, is obtained within the LCOAO model. The theoretical analysis reveals a strong breakdown of the alternant pairing symmetry for benzo[*a*]pyrene, compared with those observed in the related hydrocarbons benz[*a*]anthracene and chrysene.

## Introduction

Benzo[*a*]pyrene (BaP), a widespread environmental contaminant and a potent carcinogen, has long been among the most extensively investigated polycyclic benzenoid hydrocarbons.[1] It is thus remarkable that essential features of the electronic structure of BaP remain incompletely elucidated. For example, little seems to be known about the polarization directions of its electronic transitions, although this information is of importance in the study of several aspects of its biological reactivity.[2-4]

In the present investigation we study the electronic spectrum of BaP by experimental and theoretical methods, using a similar approach as in our recent investigations of chrysene[5] and benz[*a*]anthracene[6,7] and a number of derivatives and related com-

Chart I. Benzo[*a*]pyrene (BaP)

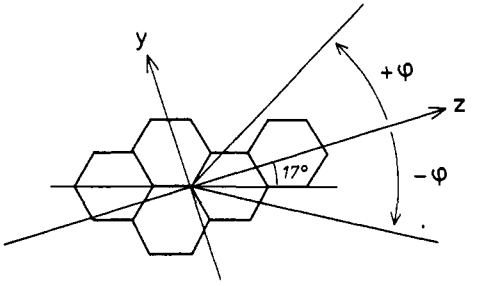


† Roskilde University.
‡ Polish Academy of Sciences.
§ Chalmers University of Technology.
⊥ The World Bank.

0002-7863/92/1514-1942$03.00/0 

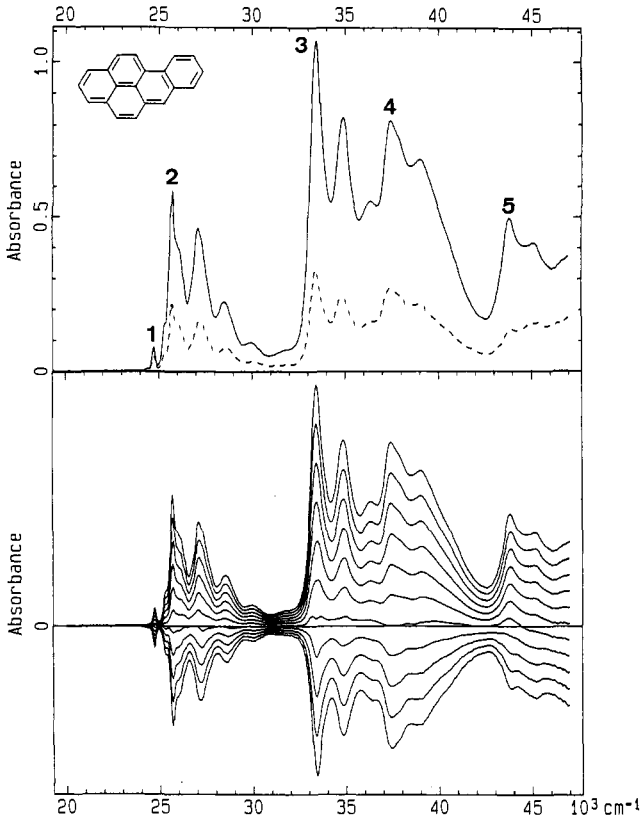


**Figure 1.** Top: Linear dichroic absorption curves for benzo[*a*]pyrene aligned in stretched polyethylene at room temperature. The figure shows $E_Z(\tilde{\nu})$ (full line) and $E_Y(\tilde{\nu})$ (broken line) obtained with the electric vector of the polarized light parallel and perpendicular, respectively, to the stretching direction of the sample. Bottom: Reduced absorption curves $r_K(\tilde{\nu}) = (1 - K)E_Z(\tilde{\nu}) - 2KE_Y\tilde{\nu}$ with $K$ ranging from 0 to 1 in steps of 0.1.

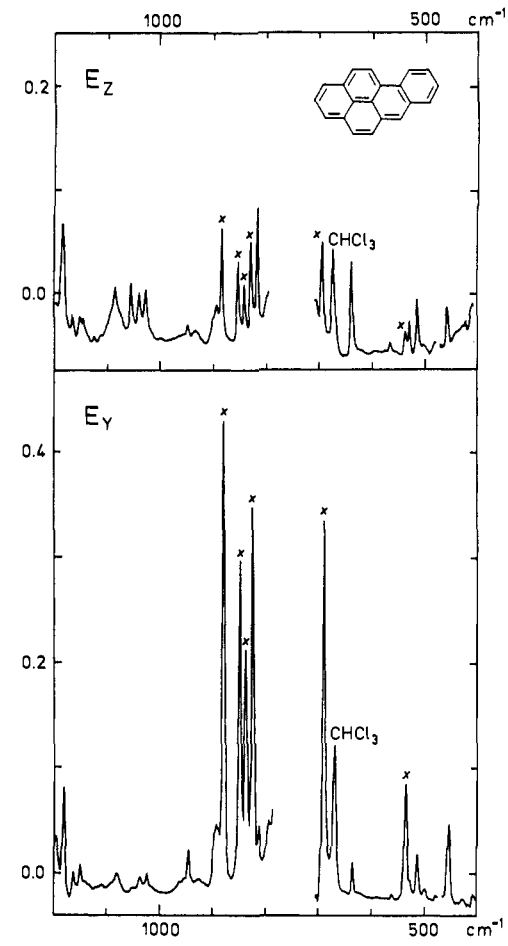


**Figure 2.** Linear dichroic IR absorption curves $E_Z(\tilde{\nu})$ and $E_Y(\tilde{\nu})$ for benzo[*a*]pyrene aligned in stretched polyethylene at room temperature, with indication of the assignment of strong out-of-plane ($x$) polarized vibrational transitions.

pounds.[8] This approach combines the information from UV and IR linear dichroism (LD), fluorescence polarization, and magnetic circular dichroism (MCD) spectroscopy with that from quantum chemical calculations using several semiempirical procedures. The result is a detailed characterization of transitions in the near-UV region, including precise determination of electronic transition moment directions.[5-8]

Stretched polyethylene has turned out to be extremely useful as an anisotropic solvent in LD spectroscopy on aromatic hydrocarbons and many other compounds.[9-14] Even molecules with near-spherical shape may be partially aligned in stretched polyethylene (see, e.g., ref 15), which allows for both IR and UV LD spectroscopy. The LD spectra provide information on molecular alignment as well as on transition moment directions. This information frequently allows conclusions concerning molecular geometry.[11-16] It also often leads to detection of otherwise "hidden" transitions, for instance in the case of pyrene[9-11] and chrysene.[5]

## Experimental Section

A sample of BaP was obtained from commercial sources (Aldrich), and the spectroscopic purity of the compound was checked by comparison of its absorption and fluorescence spectra with literature data.[17]

(1) Osborne, M. R.; Crosby, N. T. *Benzopyrenes*; Cambridge Monographs on Cancer Research; Coombs, M. M., Ashby, J., Newbold, R. F., Baxter, H., Eds.; Cambridge University Press: Cambridge, England, 1987.

(2) Nordén, B.; Kubista, M. In *Polarized Spectroscopy of Ordered Systems*; Samori, B., Thulstrup, E. W., Eds.; Nato ASI Series C; Kluwer Academic: Dordrecht, The Netherlands, 1988; Vol. 242, pp 133–165.

(3) Undemann, O.; Lycksell, P.-O.; Gräslund, A.; Astlind, T.; Ehrenberg, A.; Jernström, B.; Tjerneld, F.; Nordén, B. *Cancer Res.* **1983**, *43*, 1851. Eriksson, M.; Jernström, B.; Gräslund, A.; Nordén, B. *J. Chem. Soc., Chem. Commun.* **1986**, 1613. Eriksson, M.; Nordén, B.; Jernström, B.; Gräslund, A. *Biochemistry* **1988**, *27*, 1213. Eriksson, S.; Jernström, B.; Nielsen, P. E.; Nordén, B. *FEBS Lett.* **1989**, *248*, 201; Eriksson, M.; Eriksson, S.; Nordén, B.; Jernström, B.; Gräslund, A. *Biopolymers* **1990**, *29*, 1249.

(4) Nagata, C.; Kodama, M.; Tagashira, Y.; Imamura, A. *Biopolymers* **1966**, *4*, 409. Green, B.; McCarter, J. A. *J. Mol. Biol.* **1967**, *29*, 447. Li, K. P.; Glick, M. R.; Indralingam, R.; Winefordner, J. D. *Spectrochim. Acta* **1989**, *45A*, 471.

(5) Spanget-Larsen, J.; Waluk, J.; Thulstrup, E. W. *J. Phys. Chem.* **1990**, *94*, 1800; *Erratum* **1990**, *94*, 6926.

(6) Waluk, J.; Thulstrup, E. W. *Chem. Phys. Lett.* **1987**, *135*, 515.

(7) Waluk, J.; Mordziński, A.; Spanget-Larsen, J.; Thulstrup, E. W. *Chem. Phys.* **1987**, *116*, 411.

(8) Waluk, J.; Mordziński, A.; Spanget-Larsen, J.; Thulstrup, E. W. *Chem. Phys.* **1988**, *124*, 103. Waluk, J.; Thulstrup, E. W. *Spectrochim. Acta* **1988**, *44A*, 1335.

(9) Thulstrup, E. W.; Eggers, J. H. *Chem. Phys. Lett.* **1968**, *1*, 690. Thulstrup, E. W.; Michl, J.; Eggers, J. *J. Phys. Chem.* **1970**, *74*, 3868. Michl, J.; Thulstrup, E. W.; Eggers, J. *J. Phys. Chem.* **1970**, *74*, 3878.

(10) Thulstrup, E. W. *Aspects of the Linear and Magnetic Circular Dichroism of Planar Organic Molecules*; Springer-Verlag: Heidelberg, FRG, 1980.

(11) Michl, J.; Thulstrup, E. W. *Spectroscopy with Polarized Light. Solute Alignment by Photoselection, in Liquid Crystals, Polymers, and Membranes*; VCH: New York, 1986.

(12) Thulstrup, E. W.; Michl, J. *Acta Phys. Pol.* **1987**, *A71*, 839; *Spectrochim. Acta* **1988**, *44A*, 767. Michl, J.; Thulstrup, E. W. *Acc. Chem. Res.* **1987**, *20*, 192.

(13) Radziszewski, J. G.; Michl, J. *J. Am. Chem. Soc.* **1986**, *108*, 3289. Radziszewski, J. G.; Arrington, C. A.; Downing, J. W.; Balaji, V.; Murthy, G. S.; Michl, J. *J. Mol. Struct. (Theochem)* **1988**, *163*, 191.

(14) Thulstrup, E. W.; Michl, J. *Elementary Polarization Spectroscopy*; VCH: New York, 1989.

(15) Spanget-Larsen, J.; Uschmann, J.; Gleiter, R. *J. Phys. Chem.* **1990**, *94*, 2334. Spanget-Larsen, J.; Gleiter, R.; Haider, R. *Helv. Chim. Acta* **1983**, *66*, 1441.

(16) Spanget-Larsen, J.; Fink, N. *J. Phys. Chem.* **1990**, *94*, 8423. Herbich, J.; Rotkiewicz, K.; Waluk, J.; Andresen, B.; Thulstrup, E. W. *Chem. Phys.* **1989**, *138*, 105.

(17) (a) Heinrich, G.; Güsten, H. In *Polynuclear Aromatic Compounds*; Bjørseth, A., Dennis, A. J., Eds.; Battelle: Columbus, OH, 1980; pp 983–1003. (b) Van den Bogaardt, P. A. M.; Rettschnick, R. P. H.; Van Voorst, J. D. W. *Chem. Phys. Lett.* **1973**, *18*, 351.

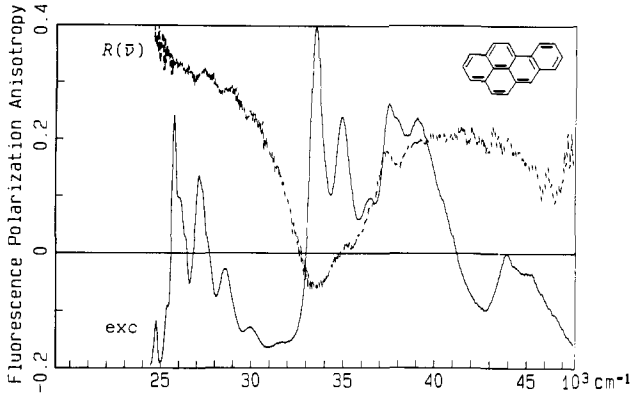


**Figure 3.** Isotropic fluorescence excitation spectrum (full line, arbitrary scale) and degree of fluorescence polarization anisotropy $R(\tilde{\nu})$ (broken line) for benzo[*a*]pyrene in a 1,2-propanediol glass at 200 K.

**Table I.** Observed Wave Numbers $\tilde{\nu}_i$ ($10^{-3}$ cm$^{-1}$), Orientation Factors $K_i$, Fluorescence Polarization Anisotropies $R_i$, and Transition Moment Angles $\phi_i$ (deg) for Peaks in the Spectrum of Benzo[*a*]pyrene

| electronic transition[a] | $\tilde{\nu}_i$ | $K_i$ | $R_i$ | $\lvert\phi_i\rvert$[b] | $\lvert\phi_1 - \phi_i\rvert$[c] | $\phi_i$[d] |
|---|---|---|---|---|---|---|
| 1 | 24.8 | 0.45 ± 1[e] | | 45 | | −45 ± 1[f] |
| 2 | 25.8 | 0.56 ± 2 | +0.35 | 30 | 17 | −30 ± 3 |
| | 27.2 | | | | | |
| | 28.6 | | | | | |
| | 30.0 | | | | | |
| 3 | 33.5 | 0.63 ± 2 | −0.06 | 18 | 61 | +18 ± 4 |
| | 34.9 | | | | | |
| | 36.4 | | | | | |
| 4 | 37.5 | 0.56 ± 3 | +0.20 | 30 | 35[g] | −30 ± 4 |
| | 39.0 | | | | | |
| 5 | 43.9 | 0.70 ± 3 | +0.20 | 0 | 35[g] | 0 ± 15 |
| 6? | 45.3 | 0.60 ± 5 | +0.13 | 23 | 42[g] | ±23 ± 10 |

[a] Assignment of individual electronic transitions. [b] Absolute $\phi_i$ values derived from the observed $K_i$ values using (3). $\phi_i$ is defined in Chart I. [c] Relative $\phi_i$ values from the observed $R_i$ values using (5). [d] For determination of sign, see text. [e] Experimental error limits in units of 0.01. [f] Error limits based on the uncertainty of $K_i$ values. [g] These values are probably inaccurate because of band overlap.

LD spectra were measured in uniaxially stretched (400%) polyethylene (PE) sheets. The samples for the UV measurements were prepared from 100-μm PE film material (Panther Plast A/S, Vordingborg, Denmark). For the IR spectra, material cut from a laboratory bottle made of ~2-mm-thick pure PE was used (Kartell, FRG). The samples were prepared as previously described.[5]

The near-UV LD spectra were recorded on a Shimadzu Model MPS-2000 spectrophotometer equipped with rotatable Glan prism polarizers as described previously.[5,18] The observed base-line-corrected UV LD absorption curves obtained at room temperature with a slit width of 0.5 nm are shown in Figure 1.

IR LD spectra[13] were measured as previously described on a Perkin-Elmer Model 1710 FTIR instrument equipped with a SPECAC Model KRS-5 polarizer.[5] The spectra were recorded at room temperature as the average of 10 scans with a spectral resolution of 4 cm$^{-1}$. The observed base-line-corrected IR LD absorption curves for BaP in the 400–1200-cm$^{-1}$ region are shown in Figure 2; the blank region between 700 and 800 cm$^{-1}$ could not be investigated because of strong absorption due to polyethylene and traces of chloroform.

Fluorescence polarization[11,14] measurements were performed using an Aminco Model SPF-500 spectrofluorometer and an Oxford Instruments Model DN1704 cryostat. A prism polarizer was used for the excitation and a Polaroid sheet for the emission. Polarized excitation[11,14] spectra were recorded from a ~$10^{-5}$ M solution of BaP in a 1,2-propanediol glass at 200 K with an excitation bandwidth of 2 nm. The fluorescence was monitored at 410 nm with a bandwidth of 5 nm; the anomalous fluorescence observed at room temperature and assigned[17b] to emission from $S_2$ and from a vibrationally excited $S_1$ was negligible in the present low-temperature spectrum. The isotropic fluorescence excitation spectrum and the observed degree of fluorescence polarization anisotropy

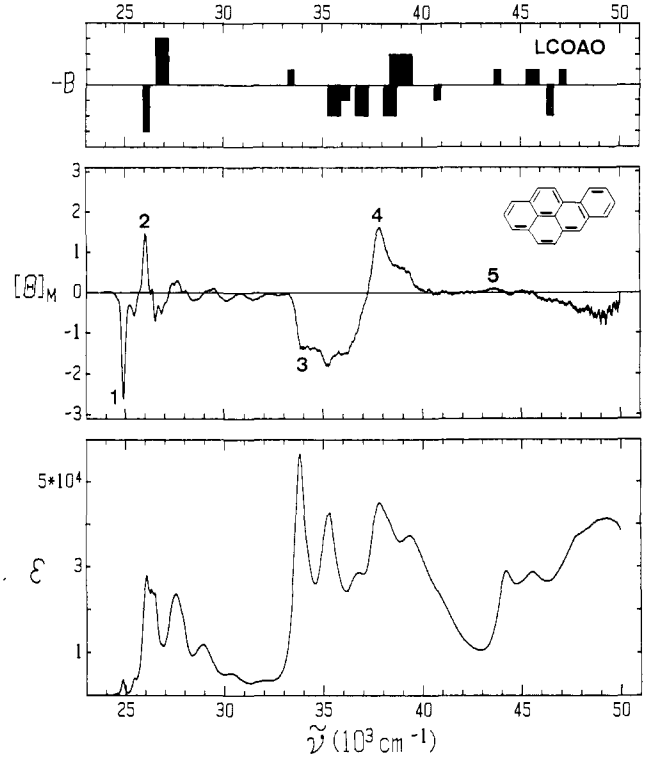


**Figure 4.** Top: Graphical representation of $S_n \leftarrow S_0$ transitions in benzo[*a*]pyrene calculated by the LCOAO method (Table II). The thickness and length, respectively, of the bars correspond to different values of oscillator strengths $f$ ($f < 0.1$, $0.1 < f < 1$, $1 < f$) and MCD $B$ terms ($|B| < 1$, $1 < |B| < 5$, $5 < |B|$). Center: Observed MCD spectrum of BaP in heptane at room temperature (positive MCD corresponds to negative $B$ term and vice versa). Bottom: Observed absorption spectrum of BaP in heptane at room temperature.

$R(\tilde{\nu})$[11,14] are shown in Figure 3; $R_i$ values for selected peaks $i$ are included in Table I.

The MCD[10] spectrum of BaP in *n*-heptane (Merck, spectral quality) was measured at room temperature on a Jasco Model J-600 spectropolarimeter equipped with a 16-kG electromagnet.[5] The recorded MCD spectrum is shown in Figure 4, and the extracted MCD $B$ terms[10] are listed in Table II. The observed data are consistent with the results of Yamaguchi et al.[19] who measured the MCD spectrum of BaP in the 22000–40000-cm$^{-1}$ region.

## Calculations

The electronic transitions of BaP were calculated with the PPP[20] π-electron model and by the CNDO/S,[21,22] CNDO-SDCI,[22] and LCOAO[23,24] all-valence-electrons procedures. The results are listed in Tables II and III.

The PPP calculation was based on a regular hexagon geometry with a standard bond length of 1.4 Å. The parameters were taken as $\beta^\circ = -2.318$ eV and $\gamma_{\mu\nu} = (14.398 \text{ eV})/[1.328 + (R_{\mu\nu} (\text{Å}))]$.[20b] The 64 monoexcited singlet configurations generated by promotion of electrons from the 8 highest π to the 8 lowest π* molecular orbitals (MO's) were included in the configuration interaction (CI) procedure.

The all-valence-electrons calculations used the experimental geometry of BaP as determined by X-ray crystallography[25] (the

(18) Myrvold, B. O.; Spanget-Larsen, J.; Thulstrup, E. W. *Chem. Phys.* **1986**, *104*, 305.

(19) Yamaguchi, H.; Tateishi, M.; Muraoka, T. *Spectrochim. Acta* **1980**, *36A*, 229.

(20) (a) Pariser, R.; Parr, R. G. *J. Chem. Phys.* **1953**, *21*, 466. Pople, J. A. *Trans. Faraday Soc.* **1953**, *49*, 1375. (b) Nishimoto, K.; Mataga, N. Z. *Phys. Chem.* **1957**, *12*, 335; *13*, 140.

(21) Del Bene, J.; Jaffé, H. H. *J. Chem. Phys.* **1968**, *48*, 1807.

(22) Baumann, H.; Oth, J. F. M. *Helv. Chim. Acta* **1980**, *63*, 618. Baumann, H. *QCPE* **1977**, *10*, 333.

(23) Spanget-Larsen, J. *Theor. Chim. Acta* **1980**, *55*, 165.

(24) Spanget-Larsen, J. *Croat. Chem. Acta* **1986**, *59*, 711.

(25) Iball, J.; Scrimgeour, S. N.; Young, D. W. *Acta Crystallogr.* **1976**, *B32*, 328.

**Table II.** Calculated[a] and Observed[b] Wave Numbers $\bar{\nu}$ ($10^3$ cm$^{-1}$), Oscillator Strengths $f$, Transition Moment Angles $\phi$[c] (deg), and MCD $B$ Terms ($10^{-3}\beta_e D^2$/cm$^{-1}$) for $S_n \leftarrow S_0$ Transitions in Benzo[a]pyrene

| | | PPP[a] | | | LCOAO[a] | | | | | observed[b] | | | | |
|---|---|---|---|---|---|---|---|---|---|---|---|---|---|---|
| | term | $\bar{\nu}$ | $f$ | $\phi$ | $\bar{\nu}$ | $f$ | $\phi$ | $B$ | | band | $\bar{\nu}$[d] | $f$[e] | $\phi$ | $B$ |
| 1 | $^1A'^-$ ($L_b$) | 26.4 | | | 26.1 | 0.02 | −44 | +5.1 | | 1 | 24.8 | 0.01 | −45 | +1.00 |
| 2 | $^1A'^+$ ($L_a$) | 25.1 | 0.95 | −28 | 26.9 | 0.61 | −34 | −5.4 | | 2 | 25.8 | 0.3 | −30 | −0.42[f] |
| 3 | $^1A'^-$ | 33.6 | | | 33.4 | $10^{-3}$ | −53 | −0.1 | | | | | | |
| 4 | $^1A'^+$ | 34.0 | 0.05 | +32 | 35.6 | 0.10 | +24 | +3.0 | | | | | | |
| 5 | $^1A'^+$ ($B_b$) | 35.4 | 0.82 | +28 | 35.9 | 1.53 | +19 | +0.3 | +8.2 | 3 | 33.5 | 0.6 | +18 | +4.0 |
| 6 | $^1A'^-$ | 35.2 | | | 37.0 | 0.10 | +25 | +1.6 | | | | | | |
| 7 | $^1A'^+$ | 38.0 | 0.70 | +36 | 38.4 | 0.11 | +59 | +3.4 | | | | | | |
| 8 | $^1A'^-$ | 36.9 | | | 38.5 | 0.04 | +70 | −3.8 | | | | | | |
| 9 | $^1A'^+$ ($B_a$) | 41.4 | 1.06 | −22 | 39.0 | 1.31 | −27 | −3.8 | −7.6 | 4 | 37.5 | 0.7 | −30 | −1.5 |
| 10 | $^1A'^-$ | 41.7 | | | 40.8 | 0.01 | +9 | +0.2 | | | | | | |
| 11 | $^1A'^-$ | 43.5 | | | 43.8 | 0.04 | −24 | −0.4 | | | | | | |
| 12 | $^1A'^+$ | 44.5 | 0.02 | −32 | 45.6 | 0.14 | −19 | −0.9 | | 5 | 43.9 | 0.2 | ~0 | −0.1 |
| 13 | $^1A'^-$ | 44.7 | | | 46.5 | 0.05 | −21 | +2.0 | | | | | | |
| 14 | $^1A'^+$ | 46.3 | 0.37 | −28 | 47.1 | 0.02 | +11 | −0.9 | | | | | | |

[a] For calculational details, see the text. [b] See Table I. [c] $\phi$ is defined in Chart I. [d] Onset. [e] Roughly estimated values. [f] $B$ term corresponding to the onset of band 2. Integration over the range 25 600–33 000 cm$^{-1}$ yields the value +0.15 (see Figure 2).

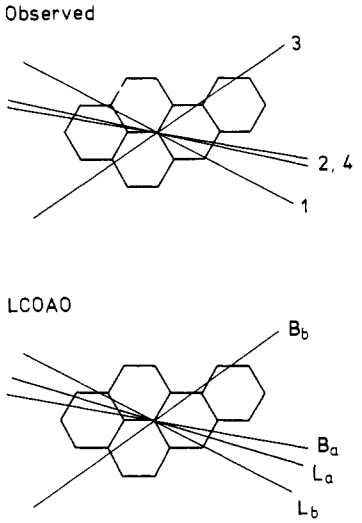


**Figure 5.** Top: Observed transition moment directions for bands 1–4 in the UV spectrum of benzo[a]pyrene. Bottom: Moment directions predicted by the LCOAO method for L- and B-type electronic transitions in BaP (Table II).

C–H bond lengths were taken as 1.09 Å). The CNDOS and CNDO-SDCI calculations were performed as previously described.[5,26] The lowering of the CNDO-SDCI ground-state energy due to the inclusion of doubly excited configurations in this model is not included in the CNDO-SDCI transition energies listed in Table III.

The LCOAO (linear combination of orthogonalized atomic orbitals) theory was developed and parametrized with particular emphasis on a satisfactory description of the observed pairing properties for alternant conjugated hydrocarbons and their radical ions.[23,24,27] The procedure is parametrized in such a manner that the next-nearest-neighbor resonance integral $\beta_{13}$ between Löwdin-orthogonalized[28] $\pi$ atomic orbitals just vanishes in the six-membered ring of benzene,[24] thereby ensuring near-perfect pairing symmetry[29] for polycyclic benzenoid hydrocarbons.[5,7,24,27] Within this treatment, MCD $B$ terms[10] for $\pi$–$\pi^*$ transitions were calculated with a perturbation procedure similar to that of Warnick and Michl;[30,31] the origin of the molecular coordinate system was taken as the center of gravity of the ground-state $\pi$-electron distribution. A series of CI calculations were performed,

**Table III.** $S_n \leftarrow S_0$ Transitions in Benzo[a]pyrene Predicted by the CNDO/S and CNDO-SDCI Procedures[a]

| | CNDO/S | | | CNDO-SDCI | | |
|---|---|---|---|---|---|---|
| $n$ | $\bar{\nu}$ | $f$ | $\phi$ | $\bar{\nu}$ | $f$ | $\phi$ |
| 1 ($L_b$) | 27.7 | 0.02 | −62 | 26.6 | 0.01 | −67 |
| 2 ($L_a$) | 27.8 | 0.36 | −31 | 26.8 | 0.39 | −32 |
| 3 | 36.6 | 0.08 | +18 | 31.9[b] | 0.001 | +45 |
| 4 | 34.3 | 0.003 | +17 | 34.2 | 0.006 | −63 |
| 5 ($B_a$) | 37.5 | 0.71 | +23 | 35.7 | 0.73 | +22 |
| 6 | 37.0 | 0.15 | +15 | 36.1 | 0.02 | +31 |
| 7 | 39.8 | $10^{-4}$ | +74 | 38.2[c] | 0.005 | −11 |
| 8 | 40.2 | 0.05 | +72 | 38.7 | 0.17 | +25 |
| 9 ($B_b$) | 40.7 | 0.56 | −32 | 39.9 | 0.54 | −31 |
| 10 | 42.7 | 0.02 | −54 | 40.5 | 0.01 | −24 |
| 11 | 43.3 | 0.03 | −33 | 40.8 | 0.006 | +49 |
| 12 | 46.1 | 0.004 | +15 | 42.0 | 0.002 | +22 |
| 13 | 48.3 | 0.05 | −38 | 44.3[d] | 0.04 | −37 |
| 14 | 47.5 | 0.008 | +13 | 45.2 | 0.01 | −12 |

[a] For calculational details, see text. [b] 23% doubly excited character (20% $|1,1 \rightarrow -1,-1\rangle$). [c] 12% doubly excited character. [d] 40% doubly excited character.

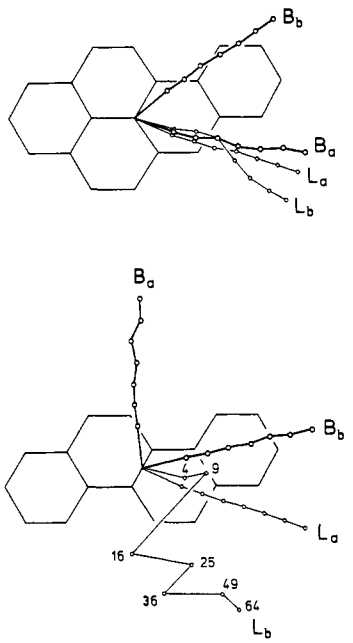


**Figure 6.** Graphical illustration of computed moment directions for L- and B-type electronic transitions in benzo[a]pyrene (top) and chrysene (bottom) as a function of the CI expansion. The figure indicates the results of LCOAO calculations with inclusion of 4, 9, 16, 25, 36, 49, or 64 monoexcited configurations in the CI, corresponding to promotion of electrons from the $N$ highest $\pi$ to the $N$ lowest $\pi^*$ MO's with $N$ ranging from 2 to 8.

(26) Spanget-Larsen, J.; Gleiter, R. *Helv. Chim. Acta* **1978**, *61*, 2999.
(27) (a) Spanget-Larsen, J. *Croat. Chem. Acta* **1984**, *57*, 991. (b) Höweler, U.; Spanget-Larsen, J.; Michl, J. To be published.
(28) Löwdin, P.-O. *J. Chem. Phys.* **1950**, *18*, 365; **1953**, *21*, 496.
(29) Pariser, R. *J. Chem. Phys.* **1956**, *24*, 250.
(30) Warnick, S. M.; Michl, J. *J. Am. Chem. Soc.* **1974**, *96*, 6280.
(31) Spanget-Larsen, J. *QCPE Bull.* **1981**, *1*, 37.

considering all monoexcited configurations derived by excitation from the $N$ highest $\pi$ to the $N$ lowest $\pi^*$ MO's, with $N$ ranging from 2 to 8. The LCOAO results listed in Table II and displayed in Figures 4 and 5 are those obtained for $N = 8$, but with an energy cutoff limit of 10 eV, leading to inclusion of 54 excited configurations in the CI. The dependence of transition moment directions on the selection of configurations included is shown in Figure 6, where also results for chrysene[5] are shown.

**Linear Dichroism and Fluorescence Polarization Spectra: Transition Moment Directions**

The observed base-line-corrected UV LD absorption curves $E_Z(\tilde{\nu})$ and $E_Y(\tilde{\nu})$ are shown in Figure 1. $E_Z(\tilde{\nu})$ and $E_Y(\tilde{\nu})$ denote the spectra recorded with the electric vector of light polarized along the stretching direction of the PE sample ($Z$) and perpendicular to it ($Y$).

The orientational properties that can be determined from the experimental LD curves are the orientation factors $K_i$ for the transition moments $M_i$ of the observed transitions $i$:[9-14]

$$K_i = \langle \cos^2 (M_i,Z) \rangle \quad (1)$$

The pointed brackets indicate averaging over all molecules in the light path, and $(M_i,Z)$ is the angle between the moment of transition $i$ and the polymer stretching direction $Z$. Provided a spectral feature associated with transition $i$ can be recognized in $E_Z(\tilde{\nu})$ and $E_Y(\tilde{\nu})$, the orientation factor $K_i$ can be obtained, even in the case of overlap with absorption due to other, differently polarized transitions, by using the TEM stepwise reduction procedure.[9-14] In the present application, we form "reduced" linear combinations[5]

$$r_K(\tilde{\nu}) = (1 - K)E_Z(\tilde{\nu}) - 2KE_Y(\tilde{\nu}) \quad (2)$$

by variation of $K$ between 0 and 1. A spectral feature due to transition $i$ (a peak or a shoulder) will vanish from the linear combination $r_K(\tilde{\nu})$ for $K = K_i$.[5] A series of reduced curves based on the observed UV LD curves for BaP are shown in Figure 1, and the $K_i$ values determined by visual inspection for 12 peaks are listed in Table I.

As mentioned above, the $K_i$ value is equal to the average cosine square of the angle between the moment of transition $i$ and the stretching direction $Z$ of the polymer matrix (1). It is much less straightforward to obtain the transition moment directions with respect to the molecular framework of BaP. The molecular symmetry of BaP is $C_s$, which allows infinite possible moment directions for electric dipole allowed transitions: perpendicular to the molecular plane (e.g., $\sigma$–$\pi^*$) or along any direction in it ($\pi$–$\pi^*$).

If it is assumed that all significant spectral intensity in the near-UV region is of $\pi$–$\pi^*$ type and thus is polarized in the molecular plane, the task consists of determination of the angles $\phi_i$ formed by the moments of the observed transitions $i$ with a specific, well-defined molecular axis in the plane. We define this axis as the molecular axis $z$ corresponding to the largest value of the directional cosine square $\langle \cos^2 (z,Z) \rangle = K_z$. The molecular axis $z$ is the one that on the average is best aligned with the stretching direction $Z$ and is called the molecular orientation axis. In stretched PE, this tends to coincide with the longest in-plane molecular dimension (the "long axis").[9-14] The orientation axis $z$, the in-plane axis $y$ perpendicular to $z$, and the out-of-plane axis $x$ define a molecular coordinate system in which the orientation tensor $\mathbf{K}$ is diagonal.[10-12] The diagonal elements $K_x$, $K_y$, and $K_z$ are the orientation factors for the axes $x$, $y$, and $z$ and are called the molecular orientation factors; from their definition, it follows that $K_x \leq K_y \leq K_z$ and $K_x + K_y + K_z = 1$. For an in-plane polarized transition $i$ we now have[9-11]

$$\tan^2 \phi_i = (K_z - K_i)/(K_i - K_y) \quad (3)$$

The magnitude of the angle $\phi_i$ between the transition moment $M_i$ and the orientation axis $z$ may thus be determined, provided the molecular orientation factors $K_y$ and $K_z$ are known.

To obtain additional information on the molecular orientation factors, we have measured the IR LD spectra of BaP. Six strong vibrational transitions with $K_i$ values equal to $0.10 \pm 0.01$ were observed at 536, 690, 825, 836, 849, and 880 cm$^{-1}$. We assign these to out-of-plane ($x$) polarized transitions (Figure 2). Thus, $K_x = 0.10$, and since $K_x + K_y + K_z = 1$, we obtain $K_y + K_z = 0.90$.

The remaining observed IR transitions have $K_i$ values ranging from $0.22 \pm 0.01$ (455 and 945 cm$^{-1}$) to $0.60 \pm 0.01$ (636 and 814 cm$^{-1}$); the observed $K_i$ values for transitions in the UV region range from $0.45 \pm 0.01$ to $0.70 \pm 0.03$ (Table I). Since $K_z$ must be larger than or equal to any of the observed $K_i$ values, we have $0.70 \pm 0.03$ as a lower limit for $K_z$; i.e., $0.67 \leq K_z$. The upper limit is determined from $K_x = 0.10$ and $K_z \leq 1 - 2K_x$: $K_z \leq 0.80$. Therefore

$$0.67 \leq K_z \leq 0.80 \quad (4)$$

It is unlikely that $K_z$ is close to the higher limit since this would correspond to a rodlike orientation distribution ($K_x = K_y = 0.10$),[9-14] which seems incompatible with the molecular shape of BaP.

Further evidence is provided by the polarized fluorescence excitation spectrum. For the electronic absorption band $i$, the relative moment angle $\phi_1 - \phi_i$ is related to the degree of fluorescence anisotropy $R_i$ through the relation[11,14]

$$\cos |\phi_1 - \phi_i| = [(5R_i + 1)/3]^{1/2} \quad (5)$$

where $\phi_1$ is the angle between $z$ and the transition moment of the first (emitting) transition. The above expression is valid in the absence of depolarization effects[11,14] and provided neither the emitting state 1 nor the transition $i$ overlap with differently polarized transitions. These assumptions seem to hold in the present case for the emitting state since the $R$ value is close to the theoretical maximum (0.4) when the excitation occurs close to the onset of the longest wavelength band at 24800 cm$^{-1}$ (Figure 3). In addition, the assumption of zero band overlap seems to be fulfilled, at least to a good approximation, for the onset of transition 2 at 25 800 cm$^{-1}$ and in particular for the strong transition 3 at 33 500 cm$^{-1}$. The observed $R_i$ values for these transitions are +0.35 and –0.06, respectively, leading on the basis of (5) to the relative transition moment angles $|\phi_1 - \phi_2| = 17°$ and $|\phi_1 - \phi_3| = 61°$ (Table I).[32]

We may now determine which values of $K_z$ in the allowed range (4) are consistent with these relative moment angles. The difference $|\phi_i - \phi_j|$ between the moment angles for two transitions $i$ and $j$ is related to the orientation factors $K_y$, $K_z$, $K_i$, and $K_j$ by the expression[5,6,34]

$$\cos |\phi_i - \phi_j| = [(K_i - K_y)^{1/2}(K_j - K_y)^{1/2} \pm (K_z - K_i)^{1/2}(K_z - K_j)^{1/2}]/(K_z - K_y) \quad (6)$$

Using $K_y = 0.90 - K_z$ and the observed values $K_1 = 0.45$, $K_2 = 0.56$, and $K_3 = 0.63$ (Table I), variation of $K_z$ from 0.67 to 0.80 leads to the prediction of $|\phi_1 - \phi_2|$ values from 15° to 9° and of $|\phi_1 - \phi_3|$ values from 63° to 75°. For $K_z = 0.67$ we obtain the best agreement with $|\phi_1 - \phi_2| = 17°$ and $|\phi_1 - \phi_3| = 61°$. We shall thus assume that $K_z$ for BaP is equal to 0.67, and

$$(K_x, K_y, K_z) = (0.10, 0.23, 0.67) \quad (7)$$

These $K$ values are consistent with expectations based on molecular shape considerations.[10-14]

With $K_y = 0.23$ and $K_z = 0.67$, (3) can now be used to obtain the absolute $\phi_i$ values for the observed transitions $i$. The results are given in Table I. It may be noticed that since $K_1$ is accidentally equal to $(K_y + K_z)/2 = 0.45$, the value of $|\phi_1|$ predicted from (3)

(32) Bolotnikova et al.[33] have estimated the angle $|\phi_1 - \phi_2|$ to ~55°. It is not completely clear how this value, which is at variance with the results of the present investigation, was derived from the polarization data obtained by these authors.

(33) Bolotnikova, T. N.; Dubinin, N. V.; Zhukov, V. A.; Surin, N. M.; Utkina, L. F. *Zh. Prikl. Spektrosk. (Russ.)* **1985**, *42*, 493.

(34) An error of sign appeared in the denominator of the corresponding eq 8 in ref 5.

does not depend on the individual values of $K_y$ and $K_z$ as long as their sum is equal to 0.90, which was firmly established from LD IR spectroscopy by the observed $K_x$ value (through $K_x + K_y + K_z = 1$). The result $|\phi_1| = 45°$ is thus independent of the above arguments relating to the fluorescence polarization data.

It remains to determine the signs of the moment angles (as defined in Chart I). We first conclude that since $|\phi_1| = 45°$, $|\phi_2| = 30°$, and (from fluorescence polarization) $|\phi_1 - \phi_2| = 17°$, $\phi_1$ and $\phi_2$ must have the same sign. Similarly, $|\phi_1| = 45°$, $|\phi_3| = 18°$, and $|\phi_1 - \phi_3| = 61°$ lead to the conclusion that $\phi_3$ must have the opposite sign of $\phi_1$. The result $|\phi_1 - \phi_4| = 35°$ derived from fluorescence polarization is expected to be inaccurate because of band overlap, but with $|\phi_1| = 45°$ and $|\phi_4| = 30°$ the result is sufficient to ensure that $\phi_4$ has the same sign as $\phi_1$. The value of $\phi_5$ is relatively uncertain (Table I) but in any case so close to zero that the sign may be considered to be of minor importance.

We still have to decide whether the sequence of signs for $\phi_1$, $\phi_2$, $\phi_3$, and $\phi_4$ is +, +, −, + or −, −, +, −. The two alternatives are equally compatible with the experimental evidence. Hence, we must base the decision on a comparison with the calculated results. Only the latter sequence of signs is consistent with the calculated moment angles (Tables II and III), leading to the assignment indicated in Table I.

The results for $\phi_1$, $\phi_2$, $\phi_3$, and $\phi_4$ are shown in Figure 5 (top). It has been assumed that the orientation axis $z$ forms an angle of 17° with the long axis of the pyrene moiety of BaP, as indicated in Chart I. This assumption is essentially based on a consideration of the molecular shape of BaP and is expected to be valid within ±5°; an error in this assumption affects the absolute but not the relative moment directions.

### Observed Electronic Transitions

The low-energy region of the UV absorption spectrum of BaP is characterized by a weak transition with origin at 24 800 $cm^{-1}$, overlapping the onset of a much stronger absorption band at 25 800 $cm^{-1}$. The $\phi$ values for the two peaks at 24 800 and 25 800 $cm^{-1}$ are −45° and −30°, respectively; the first is associated with strong negative MCD (positive $B$ term) and the second with strong positive MCD (negative $B$ term). We assign these peaks to the onsets of the first two electronic transitions, 1 and 2. This assignment is consistent with previous assignments;[1] in particular, the assignment of the origin of band 2 to 25 800 $cm^{-1}$ is perfectly consistent with the results of Yamaguchi et al.[19] and Bolotnikova et al.[33] The two bands exhibit considerable vibrational fine structure and are probably influenced by vibronic interactions; this may explain the complex nature of the MCD spectrum in the region of band 2, with alternatingly positive and negative contributions (Figure 4).

The region between 33 000 and 43 000 $cm^{-1}$ is dominated by at least two overlapping intense absorption bands, 3 and 4. The peaks at 33 500, 34 900, and 36 400 $cm^{-1}$ all have $K$ values close to 0.63 and are associated with negative MCD (positive $B$ term). We assign these peaks to components of band 3. The following somewhat broader peaks at 37 500 and 39 000 $cm^{-1}$ have slightly lower $K$ values and correspond to positive features in the MCD spectrum (negative $B$ term); they are assigned to band 4. The assignments of the two overlapping transitions are supported by the fluorescence polarization results. The observed $R$ values tend to be negative in the region of band 3 and positive in the region of band 4 (Figure 3), indicating significantly different polarization directions. The transition moments of the two transitions bracket the molecular $z$ axis, with $\phi$ values equal to +18° and −30° for the onsets of band 3 and 4, resulting in similar $K$ values in spite of moment angles differing by close to 50°. Our assignment of electronic transitions in this region is at variance with the conclusions of Yamaguchi et al.,[19] as discussed in the following section of this paper.

The last band that can be observed in the stretched polyethylene spectrum is centered around 45 000 $cm^{-1}$. The observed $K$'s for the peaks at 43 900 and 45 300 $cm^{-1}$ are different (Table I), suggesting the presence of differently polarized electronic transitions. Unfortunately, neither the MCD spectrum which is very weak in this region nor the fluorescence polarization results provide further clues to the number of electronic transitions responsible for this band. The experimental evidence does not permit very precise determination of transition moment directions in the high-energy region, but the $K$ value for the peak at 43 900 $cm^{-1}$ is very close to $K_z$, indicating that this transition is essentially long-axis polarized.

### Comparison with Calculated Transitions

In the $C_s$ point group all $\pi$–$\pi^*$ transitions are allowed by the spatial molecular symmetry. But BaP is an alternant hydrocarbon, and the electronic states predicted by $\pi$-electron theories like standard PPP[20] with perfect alternant pairing symmetry can be classified as "plus" or "minus" states.[29] Electric dipole transitions from the ground state to plus states are allowed; transitions to minus states are forbidden by the pairing symmetry.[29] All-valence-electrons theories like CNDO/S, LCOAO, etc., do not contain the perfect pairing symmetry, but it is more or less closely approximated and "parity-forbidden" transitions to minus states are generally predicted to be weak. The LCOAO[23,24] procedure was designed with particular attention to a reproduction of the observed pairing properties for benzenoid hydrocarbons, and this method therefore comes close to a realization of the plus–minus symmetry for this class of compounds.

The PPP calculation on BaP predicts 14 $S_n \leftarrow S_0$ transitions below 47 000 $cm^{-1}$ (Table II), but seven of them are forbidden by the pairing symmetry in this model. Only the first of these parity-forbidden transitions, predicted at 26 400 $cm^{-1}$, seems of immediate importance. It corresponds to the $L_b$ transition in the perimeter model of Platt[35-37] ($\alpha$ according to Clar[38]). The leading contribution to the excited state wave function can be described as 89% $\{|1 \rightarrow -2\rangle - |2 \rightarrow -1\rangle\}$, where $|a \rightarrow b\rangle$ indicates a configuration derived from the ground configuration by moving one electron from orbital a to orbital b. The very weak absorption band 1 observed at 24 800 $cm^{-1}$ is assigned to this transition.

Strong parity-allowed transitions are predicted in the PPP model at 25 100, 35 400, 38 000, and 41 400 $cm^{-1}$; these would be expected to dominate the near-UV region of the absorption spectrum. From the calculation, the transitions at 25 100, 35 400, and 41 400 $cm^{-1}$ correspond to $L_a$, $B_b$, and $B_a$ transitions in the perimeter model[35-37] (p, $\beta$, and $\beta'$ according to Clar[38]). The leading contributions to the excited-state wave functions can be described as 95% $|1 \rightarrow -1\rangle$ ($L_a$), 78% $\{|1 \rightarrow -2\rangle + |2 \rightarrow -1\rangle\}$ + 13% $\{|1 \rightarrow -4\rangle + |4 \rightarrow -1\rangle\}$ ($B_b$), and 91% $|2 \rightarrow -2\rangle$ ($B_a$). The "intruder state" between the $B_b$ and $B_a$ states giving rise to the strong transition predicted at 38 000 $cm^{-1}$ is essentially 78% $\{|1 \rightarrow -3\rangle + |3 \rightarrow -1\rangle\}$ − 11% $\{|1 \rightarrow -2\rangle + |2 \rightarrow -1\rangle\}$.

Assignment of the observed absorption band 2 with maximum at 25 800 $cm^{-1}$ to the $L_a$ transition predicted at 25 100 $cm^{-1}$ is straightforward. The situation is less obvious in the case of the strong absorption between 33 000 and 43 000 $cm^{-1}$; only two intense electronic transitions are clearly observed (band 3 and 4), but PPP theory predicts *three* strong transitions in this region: the $B_b$ and $B_a$ transitions at 35 400 and 41 400 $cm^{-1}$ and the intruder at 38 000 $cm^{-1}$.

However, calculations in the all-valence-electrons models yield a significantly different picture. According to the LCOAO model (Table II), only two of the several transitions predicted between 33 000 and 43 000 $cm^{-1}$ are very strong; 90% of the absorption intensity predicted in this region is due to the $B_b$ and $B_a$ transitions. Intensity corresponding to the PPP intruder state is redistributed as a result of interactions between nominally plus and minus configurations; these interactions vanish in standard PPP theory but are significant in the all-valence-electrons models because of the breakdown of the pairing symmetry in these models (see

(35) Platt, J. R. *J. Chem. Phys.* **1949**, *17*, 484. Moffitt, W. *J. Chem. Phys.* **1954**, *22*, 320. Goutermann, M. *J. Mol. Spectrosc.* **1961**, *6*, 138.
(36) Michl, J. *J. Am. Chem. Soc.* **1978**, *100*, 6801, 6812, 6819.
(37) Klessinger, M.; Michl, J. *Lichtabsorption und Photochemie organischer Moleküle*; VCH: Weinheim, FRG, 1990.
(38) Clar, E. *Polycyclic Aromatic Hydrocarbons*; Academic Press: New York, 1964; Vols. I and II.

below). Assignment of bands 3 and 4 is now easy; although several transitions probably contribute to the absorption in this region, we may assign the two strong bands with origins at 33 500 and 37 500 $cm^{-1}$ to the $B_b$ and $B_a$ transitions predicted by the LCOAO model at 35 900 and 39 000 $cm^{-1}$, as indicated in Table II.

The assignment of the bands 1–4 to the $L_b$, $L_a$, $B_b$, and $B_a$ transitions is strongly supported by the calculated transition moment directions. The moment angles predicted by LCOAO are in perfect agreement with the observed ones within the experimental error (Table II; Figure 5). Also the PPP, CNDO/S, and CNDO-SDCI results are generally in good agreement with experiment (somewhat less so for the $L_b$ transition moment direction, see below).

The calculated MCD *B* terms are in excellent consistency with the experimental results (Table II; Figure 4), thereby further supporting the assignment of the L and B bands. The prediction of *B* terms for the transitions in the region of bands 3 and 4 is complicated by the high density of states; no less than six electronic transitions are predicted by LCOAO between 35 000 and 40 000 $cm^{-1}$. This situation is unfavorable for the application of the perturbation procedure used to compute the *B* terms.[10,30,31] Hence, the individual *B* terms computed for the several electronic transitions in this region are probably of minor significance, but it is apparent that the general structure of the MCD spectrum is well reproduced by the calculation (Figure 4).

The MCD spectrum of BaP has also been analyzed by Yamaguchi et al.,[19] but with different conclusions concerning the assignment of the electronic transitions. In particular, on the basis of a $\pi$-electron calculation, these authors assign five prominent features in absorption and MCD between 33 000 and 43 000 $cm^{-1}$ (corresponding to the peaks observed at 33 500, 34 900, 36 400, 37 500, and 39 000 $cm^{-1}$ in the present work) to five individual electronic transitions. As discussed above, we prefer the assignment of the predominant part of the intense absorption in this region to just two electronic transitions, corresponding to two vibronic series with origins at 33 500 and 37 500 $cm^{-1}$ ($B_b$ and $B_a$). The MCD spectrum in this region is of complex nature with significant contributions from several electronic transitions, but we do not believe that a detailed assignment of these contributions is possible on the basis of the information available.

In the high-energy region above 43 000 $cm^{-1}$, the agreement between calculated and observed results seems somewhat less satisfactory. Band 5 at 43 900 $cm^{-1}$ can probably be assigned to the transition predicted by LCOAO at 45 600 $cm^{-1}$, but the calculated moment direction is not in very good agreement with the observed one (Table II). The results of the CNDO-SDCI calculation indicate that the singly excited CI (SCI) picture may not be valid in this region. The state calculated by this method at 44 300 $cm^{-1}$ involves about 40% doubly excited character; in contrast, the four L and B states in the low-energy region are not significantly affected by the inclusion of doubly excited configurations (Table III).[39]

To illustrate the sensitivity of the calculated moment directions for the L and B transitions to the extension of the CI expansion within the SCI picture, the results of a series of LCOAO calculations for BaP and chrysene are shown in Figure 6. In the case of BaP, the moment directions for these transitions do not depend critically on the CI expansion; the results converge rapidly, even for the weak $L_b$ transition. This supports the conclusion that a limited CI picture is valid for the L and B states of BaP.

Results for chrysene[5] are included in Figure 6 for comparison. Here, the situation is quite different. As previously discussed,[5] the $L_b$ transition moment direction predicted for chrysene is very sensitive to the extension of the CI and probably also to other details of the calculation. This is easily explained by the extreme weakness of the calculated $L_b$ transition (oscillator strength $f = 10^{-5}$). In this case, the result of an approximate calculation must obviously be interpreted with due caution.

(39) The third excited singlet state predicted by CNDO-SDCI at 31 900 $cm^{-1}$ (Table III) involves 20% $|1,1 \rightarrow -1,-1\rangle$. There is no indication that the corresponding weak transition is observed in the present spectra, but it is probably intense in two-photon spectroscopy.

**Table IV.** Relative MO Energy Differences $\Delta HL^a$ ($cm^{-1}$) and Leading Contributions to the $L_b$ State Wave Functions for Benz[*a*]anthracene (BA), Chrysene (CH), and Benzo[*a*]pyrene (BaP)[b]

| | $\Delta HL^a$ | | $L_b$ state wave function[c] | |
|---|---|---|---|---|
| compd | CNDO/S | LCOAO | CNDO/S | LCOAO |
| BA[7] | +932 | −38 | 51% *A* − 37% *B* | 45% *A* − 44% *B* |
| CH[5] | +1203 | +57 | 52% *A* − 40% *B* | 48% *A* − 46% *B* |
| BaP | +1591 | +542 | 53% *A* − 35% *B* | 49% *A* − 41% *B* |

[a] $\Delta HL = \Delta HOMO - \Delta LUMO = (\epsilon_1 - \epsilon_2) - (\epsilon_{-2} - \epsilon_{-1})$. [b] For calculational details, see the text and refs 5 and 7. [c] $A = |1 \rightarrow -2\rangle$, $B = |2 \rightarrow -1\rangle$.

The moment direction predicted by LCOAO for the $L_b$ transition of BaP is in better agreement with experiment than the results of the CNDO-type calculations; the $\phi$ values calculated by these methods (Table III) are about 20° in error.[40] This seems to be related to the more realistic description in the LCOAO model of the alternant pairing properties. An adequate description of these properties is particularly important for transitions (like $L_b$) that are near-forbidden for reasons of approximate pairing symmetry. The results of CNDO-type calculations generally do not even approximate the degeneracies required by the pairing symmetry.[5,7,24,27,36,41] This may be seen as a result of the inadequate treatment of orbital overlap[23,24,42] in these methods, which leads to the inclusion of far too large negative next-nearest-neighbour resonance integrals $\beta_{13}$.

A convenient measure of the degree of orbital pairing symmetry for an alternant $\pi$ system is given by the quantity $\Delta HL = \Delta HOMO - \Delta LUMO$,[36,37,43] where $\Delta HOMO$ is the energy difference between the two highest doubly occupied $\pi$ MO's and $\Delta LUMO$ that between the two lowest unoccupied $\pi$ MO's. In the case of perfect pairing, $\Delta HOMO$ is equal to $\Delta LUMO$; i.e., $\Delta HL = 0$. In general, exact equality of $\Delta HOMO$ and $\Delta LUMO$ will be obtained only in standard PPP and other idealized models that contain perfect pairing symmetry. $\Delta HL$ values calculated by CNDO/S and LCOAO for benz[*a*]anthracene, chrysene, and BaP are listed in Table IV.[44] The two all-valence-electrons procedures do not predict perfect pairing symmetry, but much smaller $\Delta HL$ values are predicted by the LCOAO method; this is reflected in the computed $L_b$ state wave function which is much closer to minus-state symmetry in the LCOAO case (Table IV). But the deviation from perfect pairing is relatively large for BaP; according to the LCOAO results, it is 1 order of magnitude larger than for the other two hydrocarbons.

As a consequence of the significant perturbation of the pairing symmetry, the intensity of the $L_b$ transition should be relatively large in the case of BaP. The oscillator strength calculated by LCOAO is 0.02 (Table II), to be compared with results in the range $10^{-4}$–$10^{-5}$ for benz[*a*]anthracene[7] and chrysene.[5] The predicted trend is consistent with the experimental data: the estimated oscillator strength for the $L_b$ band of BaP is $\sim 10^{-2}$ (Table II), which is 1 order of magnitude larger than the corresponding values for benz[*a*]anthracene[7] and chrysene.[5]

The breakdown of the pairing symmetry for BaP is also indicated by the strong MCD bands in the low-energy region. In the terminology of Michl,[36,37] BaP can be characterized as a relatively hard MCD chromophore, and in agreement with Michl's qualitative rule[36,37,43] for a positive-hard MCD chromophore ($\Delta HL$

(40) In the case of benz[*a*]anthracene the situation is particularly striking; the results of NDO (neglect of differential overlap) based procedures are systematically in error by ~80° for the $L_b$ transition, while the LCOAO prediction is in agreement with experiment.[7]

(41) Ellis, R. L.; Jaffé, H. H. *J. Mol. Spectrosc.* **1974**, *50*, 474. Jørgensen, P.; Poulsen, J. C. *J. Phys. Chem.* **1974**, *78*, 1420. Obbink, J. H.; Hezemans, A. M. F. *Chem. Phys. Lett.* **1977**, *50*, 133.

(42) De Bruijn, S. *Chem. Phys. Lett.* **1978**, *54*, 399; *Erratum* **1979**, *61*, 420; *Int. J. Quantum Chem.* **1984**, *25*, 367.

(43) Michl, J. *Chem. Phys. Lett.* **1976**, *43*, 457.

(44) A discussion of corresponding relative orbital energy differences for biphenylene, an alternant hydrocarbon that deviates significantly from perfect pairing symmetry, is given by Höweler et al.[27b]

> 0), the signs +, −, +, and − are observed for the *B* terms for the $L_b$, $L_a$, $B_b$, and $B_a$ transitions. The observed MCD signs are well reproduced also by the LCOAO calculation (Figure 4; Table II). The *B* terms predicted by LCOAO for the strong $B_b$ and $B_a$ transitions (bands 3 and 4) are the result of magnetic coupling between several near-degenerate transitions, as discussed above. But the computed *B* terms for the $L_b$ and $L_a$ transitions are due almost exclusively to their mutual magnetic mixing, leading to the prediction of large positive and negative *B* terms. The *B* terms predicted by LCOAO for the $L_b$ transitions in benz[*a*]anthracene, chrysene, and BaP are +0.09,[7] +0.11,[5] and +5.1 ($10^{-3}\beta_e D^2/cm^{-1}$), reflecting the predicted increase in hardness and consistent with the observed trend: The experimental values are estimated to +0.1,[7] +0.38,[5] and +1.00.

## Summary

The combined information from UV and IR linear dichroism, fluorescence polarization, and MCD spectroscopy and from quantum chemical calculations using several models has lead to a detailed characterization of electronic transitions in BaP. Accurate experimental transition moment directions are determined for the four dominant transitions in the region below 43 000 $cm^{-1}$. These transitions can be classified as L and B in the perimeter model, and their energies, relative intensities, moment directions, and MCD signs are well reproduced by the LCOAO calculation. According to the theoretical analysis, the perturbation of the alternant pairing symmetry of BaP is unusually large for a benzenoid hydrocarbon. The breakdown of the pairing symmetry is consistent with the observed strong MCD spectrum which corresponds to that of a positive-hard MCD chromophore (ΔHOMO > ΔLUMO).

**Acknowledgment.** We are grateful to Bengt Nordén for help with the fluorescence polarization experiments, to Josef Michl for the opportunity to use his spectropolarimeter, to Dongni Wang for measuring the LD IR spectrum, to Rolf Gleiter for providing computer time at the Universitätsrechenzentrum in Heidelberg, and to Panther Plast A/S, DK-4760 Vordingborg, for a gift of pure polyethylene. Financial support from the Danish Natural Science Research Council is gratefully acknowledged.

**Registry No.** Benzo[*a*]pyrene, 50-32-8.

# Vibrational Coupling between Ethylidyne Species on Platinum Particles

**Dilip K. Paul, Thomas P. Beebe, Jr.,† Kevin J. Uram, and John T. Yates, Jr.***

*Contribution from the Surface Science Center, Department of Chemistry, University of Pittsburgh, Pittsburgh, Pennsylvania 15260.* *Received August 30, 1991*

**Abstract:** Vibrational coupling between neighboring ethylidyne species adsorbed on a $Pt/Al_2O_3$ catalyst has been detected using an equimolar mixture of $^{13}CH_3C(a)$ and $^{12}CH_3C(a)$. The coupling is detected by means of the development of increased intensity sharing in the symmetric C–H deformation mode for the chemisorbed ethylidyne species as the ethylidyne coverage increases. The results indicate that ethylidyne is produced from ethylene on (111) facets of small Pt particles, rather than on random trimer Pt sites which might also exist on the catalyst. Experiments on highly dispersed Pt catalyst surfaces have failed to detect ethylidyne production.

## I. Introduction

**A. Ethylidyne as a Detector of 3-Fold Metal Atom Sites on Catalytic Surfaces.** The interaction of ethylene with the Pt group metal surfaces is of central importance in heterogeneous catalytic chemistry due to the widespread involvement of olefinic molecules in important catalytic processes.[1] Within the last several years, it has been learned that ethylene efficiently converts to the ethylidyne species $CH_3C(a)$ near 250 K on the (111) planes of the fcc Pt group metals, or on the Ru(001) surface.[2-5] Thus, ethylidyne formation is indicative of the presence on single-crystal surfaces of metal atom sites possessing 6-fold symmetry in the upper layer. This is consistent with the $sp^3$ hybridization of the nonhydrogenic C atom in $CH_3C(a)$. The identification of ethylidyne on the 6-fold symmetric single-crystal planes has been made by vibrational spectroscopy,[6,7] LEED,[8,9] and SIMS studies.[10] In addition to these direct structural methods, the analogy of adsorbed ethylidyne to the ethylidyne moiety in organometallic compounds has been well established.[11]

In addition to work on single-crystal surfaces, several studies have dealt with ethylidyne formation on supported metal catalysts.[12-18] Here, infrared spectroscopy has been the primary tool for study, and the vibrational frequencies observed agree quite well with those found on single-crystal metals and in organometallic compounds. Work on $Pd/Al_2O_3$ has shown that approximately one-third of the exposed Pd sites are capable of adsorbing $CH_3C$ species[14] and that these species are spectator species to the catalytic hydrogenation of ethylene to produce ethane.[13] Additional investigations of $Rh/Al_2O_3$, $Ru/Al_2O_3$, and

†Present address: Department of Chemistry, University of Utah, Salt Lake City, UT 84112.

(1) Horiuti, J.; Miyahara, K. *Hydrogenation of Ethylene on Metallic Catalysts*; Government Printing Office: Washington, DC, 1968; NBS-NSRDS No. 13.
(2) Steininger, H.; Ibach, H.; Lehwald, S. *Surf. Sci.* **1982**, *117*, 685.
(3) Kesmodel, L. L.; Grates, J. A. *Surf. Sci.* **1981**, *111*, L747.
(4) Koel, B. E.; Bent, B. E.; Somorjai, G. A. *Surf. Sci.* **1984**, *146*, 211.
(5) Barteau, M. A.; Broughton, J. Q.; Menzel, D. *Appl. Surf. Sci.* **1984**, *19*, 92.
(6) Ibach, H.; Hopster, H.; Sexton, B. *Appl. Surf. Sci.* **1977**, *1*, 1.
(7) Malik, I. J.; Brubaker, M. E.; Mohsin, S. B.; Trenary, M. *J. Chem. Phys.* **1987**, *87*, 5554.
(8) Kesmodel, L. L.; Baetzold, R. C.; Somorjai, G. A. *Surf. Sci.* **1977**, *66*, 299.
(9) Kesmodel, L. L.; Dubois, L. H.; Somorjai, G. A. *Chem. Phys. Lett.* **1978**, *56*, 267.
(10) Creighton, J. R.; White, J. M. *Surf. Sci.* **1983**, *129*, 327.
(11) Skinner, P.; Howard, M. W.; Oxton, I. A.; Kettle, S. F. A.; Powell, D. B.; Sheppard, N. *J. Chem. Soc., Faraday Trans. 2* **1981**, *77*, 1203.
(12) A more thorough review of these and other ethylidyne studies is given in: Beebe, T. P., Jr.; Albert, M. A.; Yates, J. T., Jr. *J. Catal.* **1985**, *96*, 1.
(13) Beebe, T. P., Jr.; Yates, J. T., Jr. *J. Am. Chem. Soc.* **1986**, *108*, 663.
(14) Beebe, T. P., Jr.; Yates, J. T., Jr. *Surf. Sci.* **1986**, *173*, L606.
(15) Beebe, T. P., Jr.; Yates, J. T., Jr. *J. Phys. Chem.* **1987**, *91*, 254.
(16) Mohsin, S. B.; Trenary, M.; Robota, H. J. *J. Phys. Chem.* **1988**, *92*, 5229.
(17) Sheppard, N.; James, D. I.; Lesiunas, A.; Prentice, J. D. *Commun. Dept. Chem. Bulg. Acad. Sci.* **1984**, *17*, 95.
(18) Lapinski, M. P.; Ekerdt, J. G. *J. Phys. Chem.* **1990**, *94*, 4599.

0002-7863/92/1514-1949$03.00/0 